Journal of Biomedical Optics 9(1), 38–46 (January/February 2004)

Seeing the invisible: the challenge of imaging vitreous

J. Sebag*
Doheny Eye Institute
University of Southern California
Huntington Beach, California 92647
E-mail: jsebag@VMRinstitute.com

Abstract. Imaging the vitreous is an attempt to view what is by design invisible. The inability to adequately image vitreous hinders a more complete understanding of its normal structure and function and how these change in aging and disease. The combined use of more than one technique could provide better imaging for investigational and clinical purposes. Past and present imaging methodologies are summarized and research and clinical techniques that are currently in development for future applications, are discussed. Dark-field slit microscopy has been used to characterize vitreous anatomy, both within the vitreous body as well as at the vitreo–retinal interface. In addition to this methodology, slit-lamp biomicroscopy; direct, indirect, and scanning laser ophthalmoscopies; ultrasonography; optical coherence tomography; magnetic resonance and Raman spectroscopies; and dynamic light-scattering methodologies for noninvasive evaluation are presented. Dark-field slit microscopy enables *in vitro* imaging without dehydration or tissue fixatives. Optical coherence tomography enables better *in vivo* visualization of the vitreo-retinal interface than scanning laser ophthalmoscopy and ultrasonography, but does not image the vitreous body. Dynamic light scattering can determine the average sizes of vitreous macromolecules within the vitreous body as well as possibly image the posterior vitreous cortex once detached, while Raman spectroscopy can detect altered vitreous molecules, such as glycated collagen and other proteins in diabetic vitreopathy.
[DOI: 10.1117/1.1627339]

Keywords: vitreous; imaging; dark-field microscopy; ophthalmoscopy; ultrasonography; scanning laser ophthalmoscopy; Raman spectroscopy; optical coherence tomography; dynamic light scattering.

Paper 103013 received Apr. 8, 2003; accepted for publication Jul. 1, 2003.

1 [1]Introduction

As described by Duke-Elder,[1] the theories of human anatomy that were prevalent during the mideighteenth century proposed that the vitreous is composed of ''loose and delicate filaments surrounded by fluid,'' a description that is remarkably close to present-day concepts. During the eighteenth and nineteenth centuries there were no less than four very different theories of vitreous structure. In 1741 Demours formulated the alveolar theory, claiming that there are alveoli of fluid between fibrillar structures. In 1780, Zinn proposed that the vitreous is arranged in a concentric, lamellar configuration similar to the layers of an onion. The dissections and histologic preparations of Von Pappenheim and Brucke provided evidence for this lamellar theory. The radial sector theory was proposed by Hannover in 1845. Studying coronal sections at the equator, he described a multitude of sectors that are approximately radially oriented around the central anteroposterior core that contains Cloquet's canal. Hannover likened this structure to the appearance of a cut orange. In 1848 Sir William Bowman established the fibrillar theory, which was based upon his finding microscopic fibrils, an observation that confirmed Retzius's earlier description of fibers that arose in the peripheral anterior vitreous and assumed an undulating pattern in the central vitreous, similar to a horse's tail. In 1917 the elegant histological preparations of Szent-Györgi supported these observations and introduced the concept that vitreous structure changes with age.

Unfortunately, the techniques employed in all these studies[2] were flawed by artifacts that biased the results of the investigations. As pointed out by Redslob,[2] these early histological studies employed acidic tissue fixatives that precipitated what we recognize today as the glycosaminoglycan, hyaluronan, formerly called hyaluronic acid; an effect that altered the histological imaging of the vitreous. Thus the development of slit-lamp biomicroscopy by Gullstrand in 1912 held great promise, as it was anticipated that this technique could enable imaging of the vitreous structure without the introduction of fixation artifacts. Yet, as described by Redslob,[2] a varied set of descriptions resulted over the years, ranging from a fibrous structure to sheets, ''chain-linked fences,'' and various other interpretations. This problem has even persisted in more recent investigations. Eisner[3] described ''membranelles''; Worst,[4] ''cisterns''; Sebag and Balazs,[5] ''fibers''; and Kishi and Shimizu,[6] ''pockets'' in the vitreous. The observation of these so-called ''pockets'' by the last-mentioned group was ultimately found to be an age-related

*The author has no propriety interest in the imaging technologies described herein.

1083-3668/2004/$15.00 © 2004 SPIE

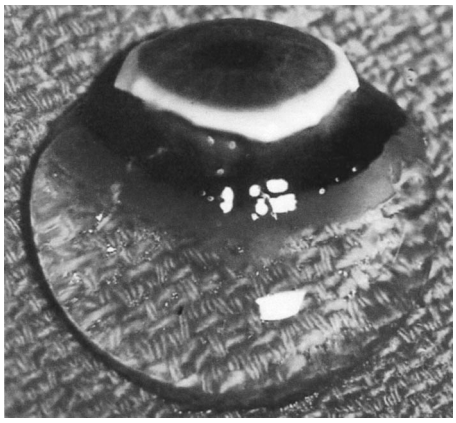

Fig. 1 Human vitreous of a 9-month-old child dissected of the sclera, choroid, and retina, still attached to the anterior segment. Although the specimen is situated on a surgical towel in room air, the vitreous maintains its shape because in youth the vitreous body is nearly entirely gel. (Specimen courtesy of the New England Eye Bank.)

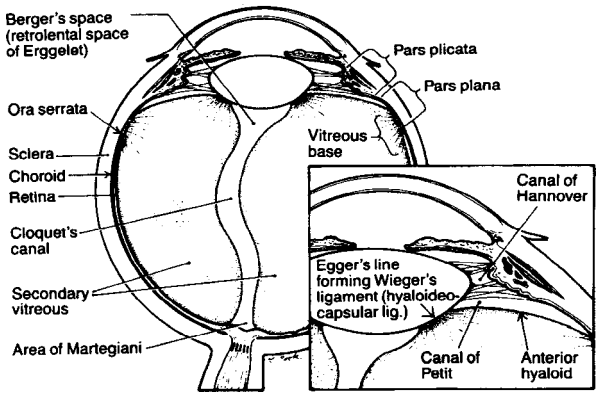

Fig. 2 Schematic diagram of "classic" vitreous anatomy.

phenomenon with little relevance to the normal macromolecular structure.[7]

Previously considered a vestigial organ, the vitreous is now regarded as an important ocular structure,[8,9] at least with respect to several important pathological conditions of the posterior segment. This remarkable tissue is in essence an extended extracellular matrix, composed largely of water, with a very small amount of structural macromolecules.[9,10] Nevertheless, in the normal state it is a solid and clear gel, especially in youth (Fig. 1). Because of the predominance of water within the vitreous, effective imaging of this structure *in vitro* is best performed by methods that overcome the intended transparency of this tissue yet avoid dehydration. Imaging the vitreous *in vivo* is must likely best achieved by visualizing the macroscopic features via an assessment of the nature and organization of the molecular components. The following discussion summarizes present concepts of vitreous structure and reviews some of the most important methods available and in development for imaging the vitreous *in vitro* and *in vivo*.

2 Vitreous Anatomy

In an emmetropic, adult human eye, the vitreous body (Fig. 2) is approximately 16.5 mm in axial length, with a depression anteriorly just behind the lens known as the patellar fossa. The hyaloideo-capsular ligament of Weiger is the annular region of vitreo-lenticular attachment that is 1 to 2 mm in width and 8 to 9 mm in diameter. Erggelet's or Berger's space is at the center of the hyaloideo-capsular ligament. Arising from this space and coursing posteriorly through the central vitreous is the canal of Cloquet [Fig. 2 and Fig. 3(g)], the former site of the hyaloid artery in the embryonic vitreous. What was previously the lumen of this artery is now an area devoid of collagen fibrils, surrounded by multifenestrated sheaths that were previously the basal laminae of the hyaloid artery wall. Posteriorly, Cloquet's canal opens into a funnel-shaped region anterior to the optic disk known as the area of Martegiani. A remnant of incomplete regression of the hyaloid artery can persist in this location and is called Bergmeister's papilla.

The peripheral shell of the vitreous body, known as the vitreous cortex, courses anterior and posterior to the vitreous base. The portion that courses forward and inward from the vitreous base is called the anterior vitreous cortex. The portion coursing posteriorly from the posterior border of the vitreous base is known as the posterior vitreous cortex. The posterior vitreous cortex is 100 to 110 μm thick and consists of densely packed type II collagen fibrils and other extracellular matrix components. Contrary to previous beliefs, there are no direct connections between the posterior vitreous cortex and the retina. Yet, the posterior vitreous cortex is quite adherent to the internal limiting lamina (ILL) of the retina, especially in youth.[11] The exact nature of this adhesion is not known, but most probably results from the action of the various extracellular matrix molecules found at this interface.[12]

3 Imaging the Vitreous

3.1 *In Vitro Imaging*

Dark-field slit microscopy of a whole human vitreous in the fresh, unfixed state was extensively employed by Sebag and Balazs to characterize the fibrous structure of the vitreous[13] (Fig. 3), age-related changes within the central vitreous body[14] and at the vitreoretinal interface,[11] and the effects of diabetes on the human vitreous structure.[15,16] This imaging method has successfully demonstrated the anatomy of the posterior vitreous cortex (Fig. 4) and the fibers in the anterior peripheral vitreous (Fig. 5) that transmit traction to the peripheral retina in rhegmatogenous retinal pathology. Fibers in this region also play a role in the formation of the so-called ''anterior loop'' configuration of anterior proliferative vitreoretinopathy. Pathological fibers,[16] believed to be the consequence of nonenzymatic glycation of vitreous collagen fibrils,[17] were also visualized in cases of diabetic vitreopathy (Fig. 6).

The reason that these normal and pathological structures are visible with dark-field slit microscopy is that this technique achieves a 90-deg illumination-observation angle that maximizes the Tyndall effect. One of the major challenges to *in vivo* imaging of the vitreous is the limitation imposed by the size of the pupil and the anatomy of the anterior segment, which work against achieving such a wide illumination-observation angle.

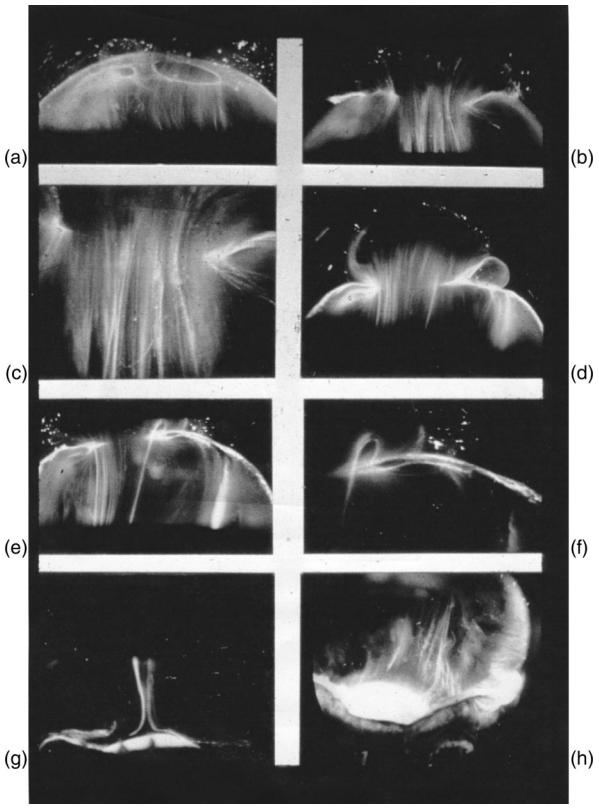

Fig. 3 Dark-field slit microscopy of human vitreous. All photographs were taken from human eyes dissected of the sclera, choroid, and retina, with the vitreous still attached to the anterior segment. The specimens were illuminated with a slit-lamp beam shown from the side and photographs were taken at a 90-*deg* angle to this plane, thereby maximizing the Tyndall effect. In all photographs the anterior segment is below and the posterior pole is above: (a) Posterior vitreous in the left eye of a 52-year old man. The corpus vitreous is "enclosed" by the vitreous cortex. There is a "hole" in the prepapillary (small hole to the left) and a dehiscence in the premacular vitreous cortex. Vitreous fibers are oriented toward the premacular vitreous cortex. (b) Posterior vitreous in a 57-year-old man. A large bundle of prominent fibers is seen coursing anteroposteriorly to exit via the premacular dehiscence in the vitreous cortex. (c) Same as (a), at higher magnification. (d) Posterior vitreous in the right eye of a 53-year-old woman. There is extrusion of the central vitreous via the prepapillary hole (to the right) in the vitreous cortex and the premacular (left) vitreous cortex. The fibers course anteroposteriorly out into the retrocortical (preretinal) space. (e) Same specimen as (d) at a different level of horizontal optical sectioning. A large fiber courses posteriorly from the central vitreous and inserts into the posterior vitreous cortex at the rim of the premacular dehiscence in the cortex. (f) Same as (e) at higher magnification. The large fiber has a curvilinear appearance because of traction by the vitreous extruding out into the retrocortical space. Because of its attachment to the vitreous cortex, the fiber arcs back to its point of insertion. (g) Anterior and central vitreous in a 33-year-old woman. The posterior aspect of the lens is seen below. Cloquet's canal is seen forming the retrolental space of Berger. (h) Anterior and peripheral vitreous in a 57-year-old man. The specimen is tilted forward to enable visualization of the posterior aspect of the lens and the peripheral anterior vitreous. Behind and to the right of the lens there are fibers coursing anteroposteriorly that insert into the vitreous base. These fibers "splay out" to insert anterior and posterior to the ora serrata.

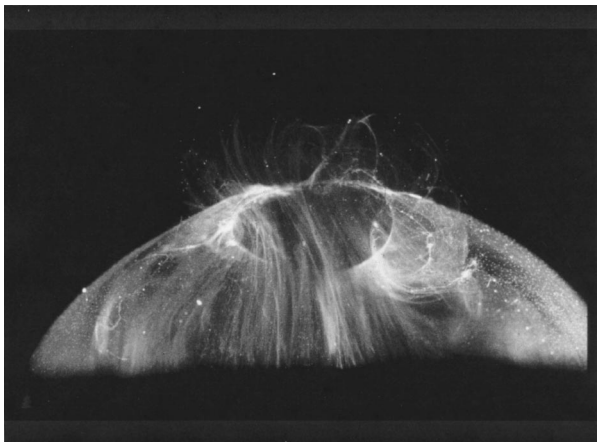

Fig. 4 Posterior and central vitreous of a 59-year-old male. The premacular hole is at the top center. Fibers course anteroposteriorly in the center of the vitreous and enter the retrocortical (preretinal) space via the premacular region of the vitreous cortex. Within the cortex are many small "dots" that scatter light intensely. The larger, irregular dots are debris. The small dots are hyalocytes.

3.2 *In Vivo Imaging*

3.2.1 *Biomicroscopy*

The effective use of slit-lamp biomicroscopy to overcome vitreous transparency necessitates maximizing the Tyndall effect. Although this can be achieved *in vitro*, as described earlier, there are limitations to the illumination-observation angle that can be achieved clinically. This is even more troublesome in the presence of meiosis, corneal and/or lenticular opacities, and limited patient cooperation. Essential to the success of achieving an adequate Tyndall effect are maximizing pupil dilation in the patient, since the Tyndall effect increases with an increasingly subtended angle between the plane of illumination and the line of observation (up to a maximum of 90 deg, as in dark-field slit-lamp microscopy *in vitro*), and dark

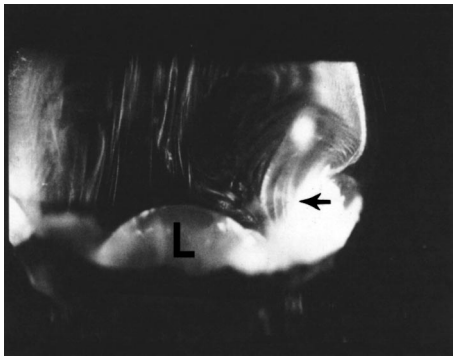

Fig. 5 Vitreous base morphology. Central and peripheral vitreous structure in a 76-year-old male. The posterior aspect of the lens (L) is seen below. Fibers course anteroposteriorly in the central vitreous and insert at the vitreous base. The "anterior loop" configuration (arrow) at the vitreous base is seen on the right side of the specimen. [Reprinted with permission from J. Sebag and E. A. Balazs, "Pathogenesis of cystoid macular edema: an anatomic consideration of vitreoretinal adhesions," *Survey of Ophthalmology* **28** (Suppl.), 493–498 (1984).]

Fig. 6 Diabetic vitreopathy. (a) Central vitreous in the left eye of a 9-year-old girl with a 5 year history of type I diabetes shows prominent fibers that resemble those seen in nondiabetic adults. (b) Peripheral vitreous of the left eye shows fibers inserting into the vitreous cortex with adjacent collections of liquid vitreous. (c) The right eye shows extrusion of the central vitreous through the posterior vitreous cortex into the retrocortical (preretinal) space. The subcortical vitreous appears very dense and scatters light intensely. Centrally, there are fibers (bottom of photo) with an anteroposterior orientation and adjacent areas of liquefaction. (d) Anterior vitreous of the right eye shows fiber insertion into the vitreous base about the lens. [Reprinted with permission from J. Sebag "Abnormalities of human vitreous structure in diabetes," *Graef's Archives of Clinical and Experimental Ophthalmology* **231**, 257, (1993).]

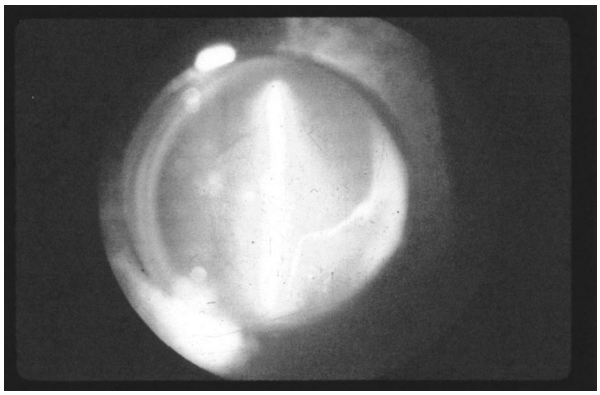

Fig. 7 Preset lens biomicroscopy of posterior vitreous detachment. The optic disk and retinal vessels are to the left; the slit beam of illumination is in the center; and the posterior vitreous cortex (linear structure to the right) can be seen detached anteriorly.

adaptation in the examiner. Some observers claim that green light enhances the Tyndall effect, although this has never been explained or tested scientifically.

Preset lens biomicroscopy slightly increases the available illumination-observation angle, offers dynamic inspection of the vitreous *in vivo*, and provides the capability of recording the findings in real time.[18] Initially introduced on a wide scale for use with a Hruby lens and currently practiced by using a hand-held 90-diopter lens at the slit lamp, this technique is purportedly best performed with a fundus camera and the El Bayadi-Kajiura lens promoted by Schepens, Trempe, and associates. This approach has been used in many seminal studies of the role of vitreous in various disease states.[18] However, there has not been widespread use of this approach, probably because it is heavily dependent upon subjective interpretation of the findings and there is thus unreliable reproducibility from facility to facility. It would be desirable to have a method of determining the presence or absence of posterior vitreous detachment (PVD) that is more objective. Furthermore, there have been no studies correlating preset lens biomicroscopy findings in patients suspected of having a posterior vitreous detachment with some type of corroborating evaluation, such as histology or intraoperative findings.

3.2.2 *Ophthalmoscopy*

Of all the parts of the eye that are routinely evaluated by clinical inspection, the vitreous is perhaps the least amenable to standard examination techniques. This is because, as previously mentioned, examining thr vitreous is an attempt to visualize a structure designed to be virtually invisible.[19] With the direct ophthalmoscope, light rays emanating from a point in the patient's fundus emerge as a parallel beam that is focused on the observer's retina and an image is formed. However, incident light reaches only the part of the fundus onto which the image of the light source falls and only light from the fundus area onto which the observer's pupil is imaged reaches that pupil. Thus the fundus can be seen only where the observed and the illuminated areas overlap and where the light source and the observer's pupil are aligned optically. This restricts the extent of the examined area. Also, because of a limited depth of field, this method is rarely used to assess the vitreous structure.

Indirect ophthalmoscopy extends the field of view by using an intermediate lens to gather rays of light from a wider area of the fundus. Although binocularity provides stereopsis, the image size is considerably smaller than with direct ophthalmoscopy and only significant alterations in vitreous structure, such as the hole in the prepapillary posterior vitreous cortex (Fig. 7) that is visible after posterior vitreous detachment, vitreous hemorrhage, or asteroid hyalosis, are reliably diagnosed by indirect ophthalmoscopy.

The scanning laser ophthalmoscope (SLO), also developed at the Schepens Eye Research Institute in Boston, enables dynamic inspection of the vitreous *in vivo*, features tremendous depth of field, and offers real-time recording of findings. Monochromatic green, as well as other wavelengths of light are also available for illumination.[20] To date, however, the SLO has really only improved our ability to visualize details in the prepapillary posterior vitreous, such as Weiss's ring (Fig. 8). In spite of the dramatic depth of field possible with this technique, the SLO does not adequately image the vitreous body and an attached posterior vitreous cortex, probably because of limitations in the level of resolution. Thus, posterior vitreous detachment, which is by far the most common diagnosis to be found when imaging the vitreous clinically, is not reliably determined by the SLO. Indeed, there is an increasing awareness among vitreous surgeons that the reliability of the clinical diagnosis of total posterior vitreous detachment by any existing technique is woefully inadequate. This awareness arises from the fact that vitreous surgery following clinical examination often reveals findings that are contradictory to preoperative assessments.

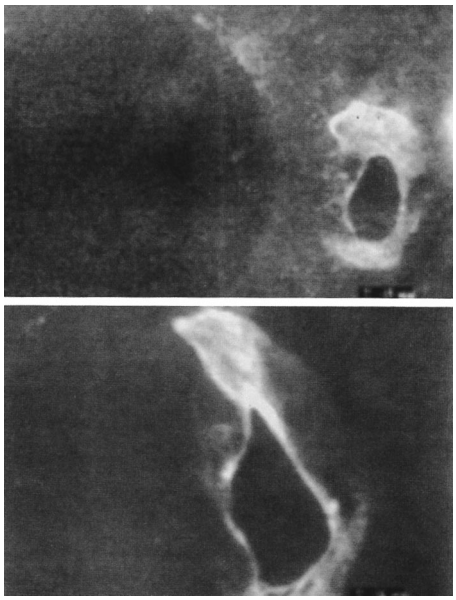

Fig. 8 Scanning laser ophthalmoscopy (SLO) of posterior vitreous. The SLO image of a detached posterior vitreous cortex demonstrates the appearance of Weiss's ring surrounding the prepapillary hole. (Reprinted with permission from Ref. 18.)

3.2.3 *Ultrasonography*

Ultrasound is an inaudible acoustic wave that has a frequency of more than 20 kHz. The frequencies used in ophthalmology are generally in the range of 8 to 10 MHz. Although these very high frequencies produce wavelengths as short as 0.2 mm, these are not short enough to adequately assess a normal internal vitreous structure such as the fibers described earlier. Even the posterior vitreous cortex, about 100 μ m at its thickest point in the normal state, is below the level of resolution of conventional ultrasonography. The utility of this technique results from the fact that strong echoes are produced at ''acoustic'' interfaces found at the junctions of media with different densities and sound velocities, and the greater the difference in density between the two media that create the acoustic interface, the more prominent the echo. Thus, age-related or pathological phase alterations within the vitreous body are detectable by ultrasonography.

Oksala, who in the late 1950s and early 1960s was among the first to employ B-scan ultrasonography to image the vitreous, summarized his findings of aging changes in 1978.[21] In that report of 444 ''normal'' subjects, Oksala defined the presence of acoustic interfaces within the vitreous body as evidence of vitreous aging and determined that the incidence of such interfaces was 5% between the ages of 21 and 40 years, and fully 80% for individuals over 60 years of age. In clinical practice, however, only relatively profound vitreous abnormalities such as asteroid hyalosis, vitreous hemorrhage, and intravitreal foreign bodies (if sufficiently large) are imaged by ultrasonography. At the vitreo–retinal interface, the presence of a posterior vitreous detachment is often suspected on the basis of B-scan ultrasonography but can never be definitively established, since the level of resolution is not sufficient to reliably image the posterior vitreous cortex, which is only a little more than 100 μ m thick at its thickest point. However,

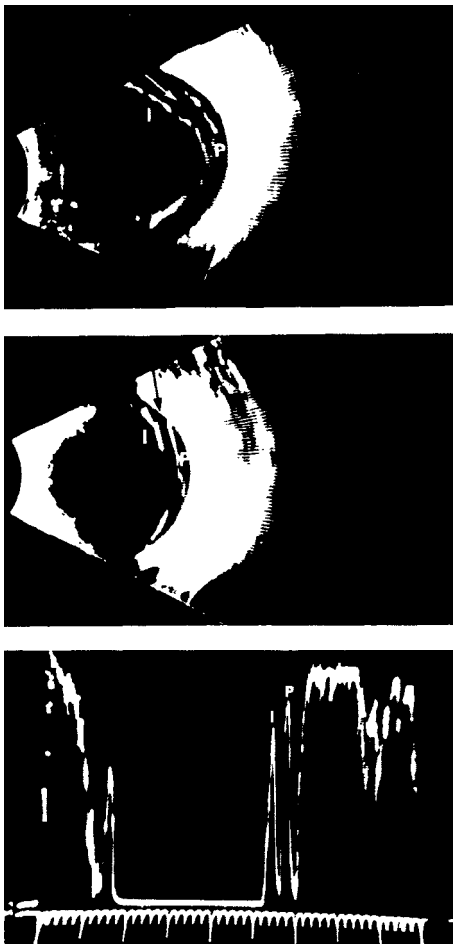

Fig. 9 Ultrasonographic imaging of vitreoschisis. Splitting of the vitreous cortex (arrow) can occur and mimic posterior vitreous detachment. In diabetic patients, blood can be present in the vitreoschisis cavity. I, inner wall; P, posterior wall of vitreoschisis cavity within the posterior vitreous cortex. (Photograph courtesy of Dr. Ronald Green. Reprinted with permission from R. L. Green and S. F. Byrne, "Diagnostic ophthalmic ultrasound," in *Retina*, S. J. Ryan, Ed., The C. V. Mosby Company, St. Louis, 1989.)

recent studies have successfully used this technique to determine the presence of a split in the posterior vitreous cortex, called vitreoschisis (Fig. 9), of patients with proliferative diabetic vitreoretinopathy.[22] The success achieved in using ultrasound to identify this important pathological entity probably results from the fact that this tissue is abnormally thickened by nonenzymatic glycation of vitreous collagen and other proteins.[22] In the absence of such advanced disease, however, the diagnosis of PVD cannot be definitively established by ultrasonography.

3.2.4 *Optical coherence tomography*

Introduced in 1991, optical coherence tomography (OCT) is a new technique for high-resolution cross-sectional imaging of ocular structure.[23] It is based on the principle of low coherence interferometry, where the distances between and sizes of structures in the eye are determined by measuring the ''echo'' time it takes for light to be backscattered from the different structures at various axial distances. The resolution of all

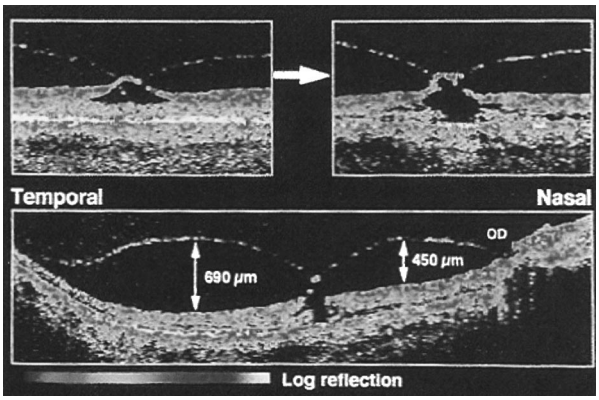

Fig. 10 Optical coherence tomography (OCT) of a macular hole. Evolution of an impending macular hole in a fellow eye to a stage II hole. (Top left) OCT shows a cystic formation in the inner part of the foveal center. The elevation of the foveal floor and the adherence of the partially detached posterior vitreous cortex suggest vitreo-retinal traction. (Top right) Two months later the roof of the cyst has opened on the nasal side of the macula, constituting an incompletely detached operculum to which the posterior vitreous cortex adheres. (Bottom) A composite optical coherence tomogram shows the convex elevation of the partially detached posterior vitreous cortex, suggesting anteroposterior vitreous traction. (Reprinted with permission from Ref. 24.)

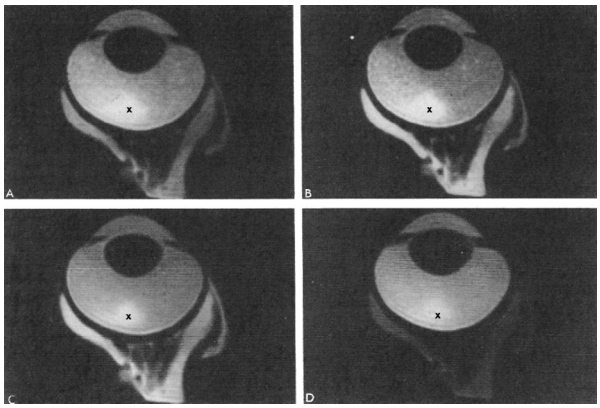

Fig. 11 NMR spectroscopy of pharmacologic vitreolysis. Progressive saturation. (a) 300 ms, (b) 1200 ms, (c) 2000 ms, (d) 3920 ms, and (e) 7864 ms images of a bovine eye 12 h after injection with 0.2 ml of 100 U/ml collagenase solution. Note the bright area (x) in the posterior pole. This area of enhanced relaxation (shorter T_1) was absent immediately after injection. In this view the optic nerve is in the edge of the plane of the image. (Reprinted with permission from Ref. 25.)

echo-based instrumentation (such as ultrasound and OCT) is based upon the ratio of the speed of the incident wave to that of the reflected wave. As described earlier, clinical ultrasonography is performed with a frequency of approximately 10 Hz and has a 150-mm resolution. Although recently introduced ultrasound biomicroscopy has increased the frequency (up to 100 Hz), and thus has a spatial resolution of 20 μm, penetration into the eye is no more than 4 to 5 mm. Light-based devices, such as the OCT, use an incident wavelength of 800 nm and have increased axial resolution to 10 μm, providing excellent imaging of retinal architecture, although vitreous applications are less useful. The limitations of OCT include the inability to obtain high-quality images through opaque media, such as dense cataract or vitreous hemorrhage. The use of OCT is also limited to cooperative patients who are able to maintain fixation for the full acquisition time of 2.5 s per section. Thus, to date OCT has primarily been used to image, and to some extent quantitate, retinal laminar structure. Some vitreous applications have been useful, especially those that involve imaging the vitreo–macular interface in patients with macular holes[24] (Fig. 10). However, the exact nature and molecular composition of these preretinal tissue planes cannot be definitively deduced using OCT, and little information can be garnered about structures within the vitreous body.

3.2.5 *Spectroscopy*

Nuclear magnetic resonance (NMR) spectroscopy. The NMR technique is based upon the fact that when placed in a magnetic field, magnetic nuclei, such as water protons, tend to orient their magnetic vectors along the direction of the magnetic field. The time constant for this orientation, known as the longitudinal relaxation time, T_1, reflects the thermal interactions of protons with their molecular environment. Magnetic vectors that have previously been induced to be in phase with each other undergo a ''dephasing'' relaxation process that is measured by the transverse relaxation time, T_2. It is the transverse relaxation time T_2 that reflects inhomogeneities within the population of protons. Protons oriented by a magnetic field absorb radio waves of a frequency appropriate to induce transactions between their two orientations. Such absorption is the basis of the NMR signal used to index relaxation times. Relaxation times in biological tissues vary with the concentration and mobility of water within the tissue. Since the latter is influenced by the interaction of water molecules with macromolecules in the tissue, this noninvasive measure can assess the gel to liquid transformation that occurs in the vitreous during aging[14] and disease states, such as diabetic vitreopathy.[15,16] These considerations led Aguayo et al.[25] to use NMR to study the effects of pharmacological vitreolysis[26,27] on bovine and human vitreous specimens and intact bovine eyes *in vitro*. Collagenase induced measurable vitreous liquefaction, more so than hyaluronidase (Fig. 11). Thus, this noninvasive method could be used to evaluate age and disease-induced synchisis (liquefaction) of the vitreous body, although it is not clear that this technique would adequately evaluate the vitreo–retinal interface. There have, curiously, been few recent studies that have employed NMR spectroscopy in research or clinical applications on the vitreous.

Raman spectroscopy. This form of spectroscopy was first described in 1928 by C. V. Raman in India. Raman spectroscopy is an inelastic light-scattering technique in which molecules in the vibrational mode in the study specimen absorb energy from incident photons, causing a downward frequency shift, which is called the Raman shift. Because the signal is relatively quite weak, current techniques employ laser-induced stimulation with gradual increases in the wavelength of the stimulating laser so as to be able to detect the points at which the Raman signal becomes apparent as peaks superimposed on the broad background fluorescence. The wavelengths at which these peaks are elicited are characteristic of

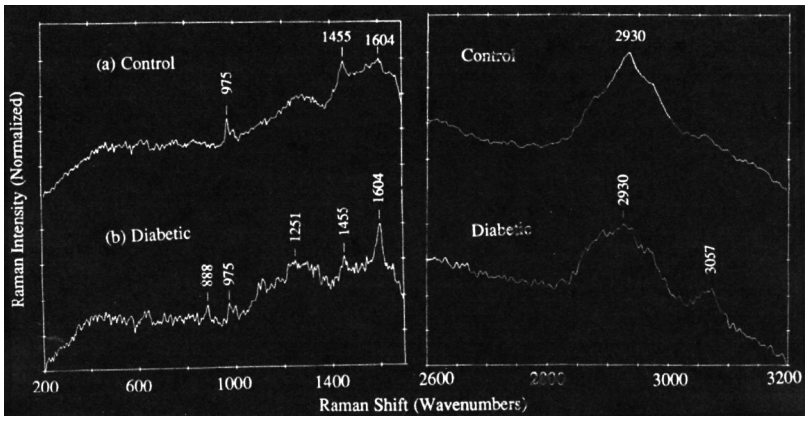

Fig. 12 Raman spectroscopy of diabetic vitreopathy. A Fourier transform of Raman spectra (FT-RS) (using a laser power of 300 mW, a laser spot diameter of 0.1 mm, and 250 co-added scans) of control and diabetic human vitreous collagen. Samples were pooled into one specimen for the patients with diabetes ($n=7$) and one for the control group ($n=10$). The graphs represent the actual FT-RS spectra of these two specimens. Quantitative analysis of the peak area at 1604 cm^{-1} showed a threefold increase in samples from patients with diabetes compared with controls. The broad background was corrected for when drawing the baseline of the peak at 1455 cm^{-1}. (Reprinted with permission from Ref. 29.)

the chemical bonds, such as aliphatic C—H (2939 cm^{-1}), water O—H (3350 cm^{-1}), C═C and C—H stretching vibrations in π-conjugated and aromatic molecules (1604 cm^{-1} and 3057 cm^{-1}), etc. To date, most applications of this technique in the eye have been for analysis of lens structure and pathology.[28] The use of near-infrared (IR) excitation wavelengths is particularly effective in the lens, since these wavelengths have better penetration in opacified cataractous lenses.

Vitreous studies[29] employed excised samples of human vitreous obtained during surgery. The near-IR excitation at 1064 nm was provided by a diode-pumped neodymium-doped: yttrium aluminum garnet (Nd:YAG) continuous wave (cw) laser with a diameter of 0.1 mm and a power setting of 300 mW. Backscattering geometry with an optical lens collected scattered light, which was passed through a Rayleigh light rejection filter into a spectrophotometer. The results (Fig. 12) showed that this technique was able to detect peaks at 1604 and 3057 cm^{-1} in the vitreous of diabetic patients that were not present in controls. Further research and development is needed to reliably interpret such results and refine the methodology for noninvasive use *in situ*. While this has already been achieved in the lens, it is not clear that this will be possible for vitreous applications.

3.2.6 *Dynamic light scattering*

Dynamic light scattering (DLS) is an established laboratory technique for measuring the average size (or size distribution) of microscopic particles as small as 3 nm in diameter that are suspended in a fluid medium where they undergo random Brownian motion. Light scattered by a laser beam passing through such a dispersion will have intensity fluctuations in proportion to the Brownian motion of the particles. Since the size of the particles influences their Brownian motion, analysis of the scattered light intensity yields a distribution of the size(s) of the suspended particles. Visible light from a laser diode (power 50 μW) is focused into a small scattering volume inside the specimen (excised lens or vitreous, autopsy or living eye). The detected signal is processed via a digital correlator to yield a time autocorrelation function (TCF). For dilute dispersions of spherical particles, the slope of the TCF provides a quick and accurate determination of the particle's translational diffusion coefficient, which can be related to its size via a Stokes-Einstein equation, provided the viscosity of the suspending fluid, its temperature, and its refractive index are known. For the lens and vitreous, a viscosity of $\eta = 0.8904$ centipoise, a refractive index of $n=1.333$, and a temperature of 25°C for *in vitro* studies and 37°C for *in vivo* studies were used to determine macromolecule sizes.

Studies[30–32] of the lens and vitreous have employed DLS instrumentation that was developed by the National Aeronautics and Space Administration to conduct fluid physics experiments on-board the space shuttle and space station orbiters. The beam input from a semiconductor laser (670-nm wavelength) at 50 μW power was projected into the specimens and the scattered signal was collected by the DLS probe for 10 s. The signal was then detected by an avalanche photodiode detector system. A TCF was constructed using a digital correlator card. The slope of the TCF provides a measure of particle sizes in the selected measurement sites (volume $=50\ \mu m^3$). Studies[31] in the lens found that DLS was significantly more sensitive than Scheimpflug photography in detecting early changes in the lens.

When the DLS probe was used to obtain measurements from the entire vitreous body, scanning was performed in conjunction with a micropositioning assembly, which controlled detector position in the x-, y-, and z-planes. This enabled semiautomated measurements from a sufficient number of sites within the bovine vitreous body to create a three-dimensional map of the distribution of the average particle sizes of vitreous macromolecules (Fig. 13). Furthermore, in studies[32] of autopsy human eyes, DLS was able to detect the structural changes[16] resulting from diabetic vitreopathy[25] (Fig. 14). It is interesting that these DLS findings appear to corroborate the findings of dark-field slit microscopy (Fig. 6) where glycation of vitreous proteins resulted in cross-linking of collagen fibrils and aggregation into large bundles of fibrils. It is plausible that these are detected by DLS as particles of larger size with more variability than that seen in the

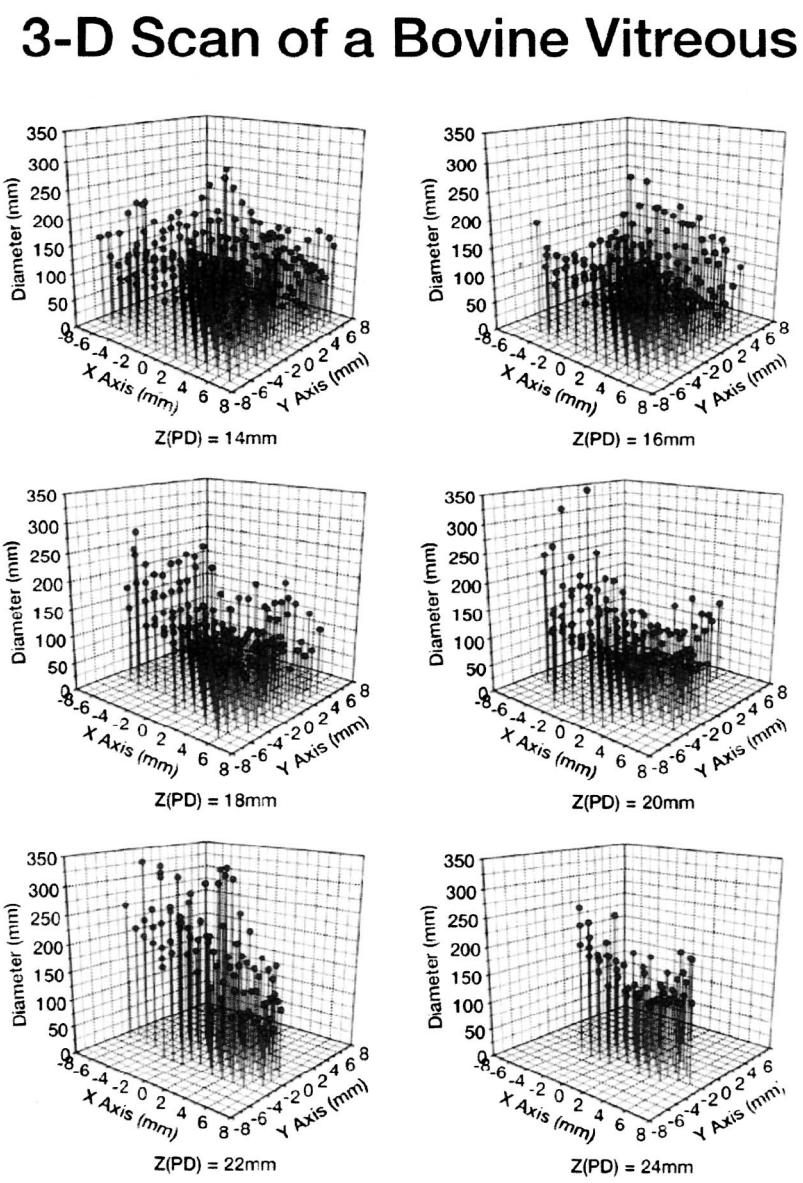

Fig. 13 Dynamic light scattering (DLS) of bovine vitreous. A three-dimensional map of DLS measurements in the bovine vitreous body *in situ*. The *x*-axis is the horizontal distance from a central (near-optical) axis of the eye. The *y*-axis is the distance along the sagittal (front-to-back) plane from the central starting point of measurements on the optical axis of the eye. From this starting point, the location of which is represented as the *z* coordinate and is defined as millimeter posterior to the lens along the optical axis in the central vitreous, measurements were obtained at 0.5-mm steps in both the x and y directions. Along the *z*-axis (in the sagittal plane), measurements were obtained every 2 mm, beginning at 14 mm behind the back surface of the lens to 24 mm posterior to this point. The heterogeneous distribution of macromolecules throughout the vitreous body can be appreciated in these plots, with the height of the lines representing the average particle size for all molecular constituents (cumulant fit of both fast hyaluronan and slow collagen) at the measurement site. (Reprinted with permission from Ref. 30.)

nondiabetic control in this preliminary study. Future studies with more advanced instrumentation will determine if this phenomenon can be detected in a clinical setting, confirming these preliminary *in vitro* results.

4 Conclusions

No single method at present exists that will provide accurate and reproducible noninvasive imaging of both the vitreous body and the vitreo–retinal interface. This significantly affects the ability to assess the effects of aging and disease and, in particular, the accuracy of clinical diagnoses of posterior vitreous detachment. Moreover, this limitation hinders our ability to adequately evaluate the role of the vitreous in vitreoretinal diseases such as retinal detachment, both in general terms and in specific clinical cases.

Today, a combination of the techniques described here could provide considerably more information than any one technique. For example, NMR spectroscopy could assess the degree of vitreous liquefaction; dynamic light scattering could determine the concurrent aggregation of collagen and other macromolecules that occurs during liquefaction; Raman spectroscopy could identify the presence of specific molecular

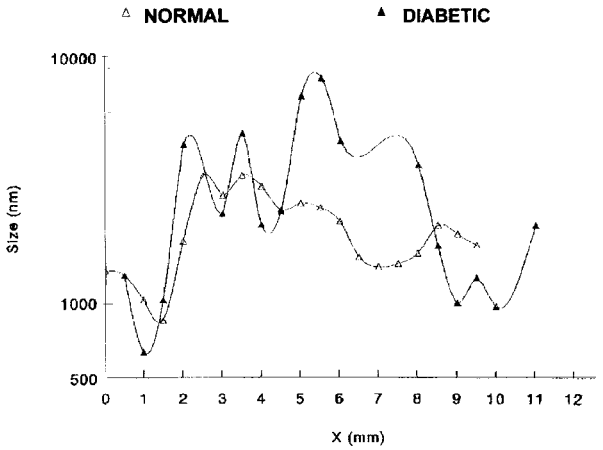

Fig. 14 Dynamic light scattering of diabetic vitreopathy. Eyes were obtained at autopsy and prepared by removing the cornea, iris, and lens from the globe, leaving the posterior capsule of the lens intact. DLS measurements were made along the anteroposterior axis at steps 0.5 mm apart, beginning behind the posterior capsule of the lens. The abscissa represents the distance from the lens capsule. The ordinate shows the particle sizes determined from the "slow component" of the time relaxation curves. In the 72-year-old patient with diabetes (solid triangles) there were larger and more varied particle sizes than in the 70-year-old nondiabetic (open triangles).

moieties that provide insight into pathogenesis; while optical coherence tomography could image the vitreo–retinal interface. It is hoped that, the future will witness the combination of these and other techniques in a single noninvasive instrument for research and clinical applications.

References

1. S. W. Duke-Elder, ''The nature of the vitreous body,'' *Br. J. Ophthamol.* (Suppl. IV) (1930).
2. E. Redslob, *Le Corps Vitre*, pp. 174–178, Societe Francaise d'Ophtalmologie Monogr., Masson, Paris (1932).
3. G. Eisner, *Biomicroscopy of the Peripheral Fundus*, Springer-Verlag, New York (1973).
4. J. G. F. Worst, ''Cisternal systems of the fully developed vitreous body in the young adult,'' *Trans. Ophthalmol. Soc. UK* **97**, 550–554 (1977).
5. J. Sebag and E. A. Balazs, ''Morphology and ultrastructure of human vitreous fibers,'' *Invest. Ophthalmol. Visual Sci.* **30**, 1867–1871 (1989).
6. S. Kishi and K. Shimizu, ''Posterior precortical vitreous pocket,'' *Arch. Ophthalmol. (Chicago)* **108**, 979 (1990).
7. J. Sebag, Letter to the editor, *Arch. Ophthalmol. (Chicago)* **190**, 1059 (1991).
8. W. S. Foulds, ''Is your vitreous really necessary? The role of the vitreous in the eye with particular reference to retinal attachment, detachment and the mode of action of vitreous substitutes'' (the second Duke-Elder Lecture), *Eye* **1**, 641–664 (1987).
9. J. Sebag, *The Vitreous: Structure, Function and Pathobiology*, Springer-Verlag, New York (1989).
10. J. Sebag, ''Macromolecular structure of vitreous,'' in *Polymer Science and the Eye*, T. V. Chirila, Ed., Progress in Polymer Science, Vol. 23, pp. 415–446 (1998).
11. J. Sebag, ''Age-related differences in the human vitreo-retinal interface,'' *Arch. Ophthalmol. (Chicago)* **109**, 966–971 (1991).
12. J. Sebag and G. S. Hageman, ''Interfaces,'' *Eur. J. Ophthalmol.* **10**, 1–3 (2000).
13. J. Sebag and E. A. Balazs, ''Human vitreous fibres and vitreoretinal disease,'' *Trans. Ophthalm. Soc. UK* **104**, 123 (1985).
14. J. Sebag, ''Age-related changes in human vitreous structure,'' *Graefe's Arch. Clin. Exp. Ophthalmol.* **225**, 89–93 (1987).
15. J. Sebag, ''Diabetic vitreopathy'' (guest editorial), *Ophthalmology* **103**, 205–206 (1996).
16. J. Sebag, ''Abnormalities of human vitreous structure in diabetes,'' *Graefe's Arch. Clin. Exp. Ophthalmol.* **231**, 257–260 (1993).
17. J. Sebag, B. Buckingham, M. A. Charles, and K. Reiser, ''Biochemical abnormalities in vitreous of humans with proliferative diabetic retinopathy,'' *Arch. Ophthalmol. (Chicago)* **110**, 1472–1479 (1992).
18. C. L. Schepens, C. L. Trempe, and M. Takahashi, *Atlas of Vitreous Biomicroscopy*, Butterworth Heinemann, Boston (1999).
19. J. Sebag, ''Classifying posterior vitreous detachment—a new way to look at the invisible,'' *Br. J. Ophthamol.* **81**, 521–522 (1997).
20. M. A. Mainster, G. T. Timberlake, R. H. Webb, and G. W. Hughes, ''Scanning laser ophthalmoscopy—clinical applications,'' *Ophthalmology* **89**, 852–857 (1982).
21. A. Oksala, ''Ultrasonic findings in the vitreous body at various ages,'' *Graefe's Arch. Clin. Exp. Ophthalmol.* **207**, 275–280 (1978).
22. T. Chu, P. F. Lopez, M. R. Cano, and R. L. Green, ''Posterior vitreoschisis—an echographic finding in proliferative diabetic retinopathy,'' *Ophthalmology* **103**, 315–322 (1996).
23. J. G. Fujimoto, M. E. Brezinski, G. J. Tearney et al., ''Optical biopsy and imaging using optical coherence tomography,'' *Nat. Med.* **1**, 970–972 (1995).
24. A. Gaudric, B. Haouchine, P. Massin et al., ''Macular hole formation—new data provided by optical coherence tomography,'' *Arch. Ophthalmol. (Chicago)* **117**, 744–751 (1999).
25. J. Aguayo, B. Glaser, A. Mildvan et al., ''Study of vitreous liquifaction by NMR spectroscopy and imaging,'' *Invest. Ophthalmol. Visual Sci.* **26**, 692–697 (1985).
26. J. Sebag, ''Pharmacologic vitreolysis,'' (guest editorial), *Retina* **18**, 1–3 (1998).
27. J. Sebag, ''Is pharmacologic vitreolysis brewing?'' (guest editorial), *Retina* **22**, 1–3 (2002).
28. S. Nie, K. L. Bergbauer, J. F. R. Kuck, Jr., and N. T. Yu, ''Near infrared Fourier transform Raman spectroscopy in human lens research,'' *Exp. Eye Res.* **51**, 619–623 (1990).
29. J. Sebag, S. Nie, K. A. Reiser, M. A. Charles, and N. T. Yu, ''Raman spectroscopy of human vitreous in proliferative diabetic retinopathy,'' *Invest. Ophthalmol. Visual Sci.* **35**, 2976–2980 (1994).
30. R. R. Ansari, S. Dunker, K. Suh, N. Kitaya, and J. Sebag, ''Quantitative molecular characterization of bovine vitreous and lens with non-invasive dynamic light scattering,'' *Exp. Eye Res.* **73**, 859–866 (2001).
31. R. R. Ansari, M. B. Datiles III, J. F. King, and D. Leftwood, ''Measuring lens opacity: combining quasi-elastic light scattering with Scheimpflug imaging system,'' *Proc. SPIE* **3246**, 35–43 (1998).
32. J. Sebag, R. R. Ansari, S. Dunker, and S. I. Suh, ''Dynamic light scattering of diabetic vitreopathy,'' *Diabetes Technol. Therap.* **1**, 169–176 (1999).